Transition to a labyrinthine phase in a driven granular medium

Simon Merminod,* Timothée Jamin, Eric Falcon, and Michael Berhanu
Université Paris Diderot, Sorbonne Paris Cité, MSC, CNRS (UMR 7057), 75013 Paris, France
(Received 8 July 2015; revised manuscript received 9 November 2015; published 11 December 2015)

Labyrinthine patterns arise in two-dimensional physical systems submitted to competing interactions, in fields ranging from solid-state physics to hydrodynamics. For systems of interacting particles, labyrinthine and stripe phases were studied in the context of colloidal particles confined into a monolayer, both numerically by means of Monte Carlo simulations and experimentally using superparamagnetic particles. Here we report an experimental observation of a labyrinthine phase in an out-of-equilibrium system constituted of macroscopic particles. Once sufficiently magnetized, they organize into short chains of particles in contact and randomly orientated. We characterize the transition from a granular gas state towards a solid labyrinthine phase, as a function of the ratio of the interaction strength to the kinetic agitation. The spatial local structure is analyzed by means of accurate particle tracking. Moreover, we explain the formation of these chains using a simple model.

DOI: 10.1103/PhysRevE.92.062205 PACS number(s): 45.70.Qj, 05.65.+b, 75.50.Kj

I. INTRODUCTION

Labyrinthine phases are intriguing two-dimensional (2D) patterns occurring in various domains of physics, in equilibrium and out-of-equilibrium situations. Two distinct phases form at small-scale well-separated stripes, which are themselves entangled, leading to a complex large-scale pattern. These shapes were experimentally obtained for extremely varied 2D systems ranging from ferrimagnetic garnet films [1] in condensed matter, Langmuir monolayers [2] in soft matter, granular fluid suspensions in which air penetrates [3,4], ferrofluid drops [5] and biphasic ferrofluid-oil layers [6] in fluid mechanics, to chemical reaction-diffusion systems [7]. The common denominator of these systems is the competition between long-range repulsion and short-range attraction, which leads to the phenomenology of modulated phases [8]. Moreover, a wide range of ordering effects that lead to different patterns can also be related to the competition between interactions and geometrical frustration, as specifically shown for magnetic thin films [9].

By analogy with the phenomenology of these continuous systems, labyrinthine and stripe phases have been introduced for systems of particles. In particular, in the context of colloidal monolayers, several Monte Carlo simulations [10–13] and one molecular dynamics simulation [14] have been performed. It was shown that, to observe stripes and labyrinthine phases, a long-range repulsive potential is needed, together with a short-range attraction, which can be replaced by a core-softened potential [10,11]. Tuning geometrical frustration in noninteracting colloidal monolayers [13,15] leads also to stripe phases. Moreover, the only experimental observation of a labyrinthine phase in a colloidal system was obtained using superparamagnetic colloids under a magnetic field, inducing dipolar interactions [16]. Labyrinthine phases were indeed found as equilibrium states at a high enough density of micrometric spheres, in agreement with dedicated Monte Carlo simulations [12,16]. In contrast, similar labyrinthine or stripe phases have not been described in a macroscopic and out-of-equilibrium system whose particles can be individually identified.

Here, we report the observation of such a labyrinthine phase. A monolayer of soft ferromagnetic spheres 1 mm in diameter is vibrated to form a 2D granular gas [17–22]. Under mechanical agitation particles undergo a Brownian-like motion, but due to the dissipative nature of the collisions, the granular gas reaches a stationary out-of-equilibrium state. Then immersed in a vertical external magnetic field B, the soft ferromagnetic spheres are magnetized and interact with each other as induced dipoles. When the magnetic field is increased, the granular gas solidifies into a phase composed of chains of a few particles in contact, similar to the labyrinthine phase observed with colloids [16]. In contrast to this colloid study, which focuses on equilibrium states, the transition from gas to labyrinth is here clearly described, using accurate particle tracking. Finally, as a remark, we emphasize that the physical mechanisms at play in labyrinthine and stripe phases of interacting particles differ from those in chain and cluster phases reported in some interacting granular gases [23–25], despite visual similarities. Indeed, these phases are composed of head-to-tail dipoles and were observed when attractive behavior is dominant at a large scale, because permanent dipoles are considered [23,25] or because the hypothesis of a quasi-2D system is not verified [24].

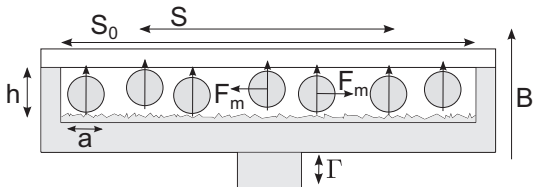

FIG. 1. Experimental setup. 5000 chromed steel spherical particles (diameter $a = 1$ mm and mass $m = 4.07$ mg) are vertically vibrated (acceleration $\Gamma = 21.9\ \mathrm{m \cdot s^{-2}}$) inside a horizontal, square aluminium cell (area $S_0 = 9 \times 9\ \mathrm{cm^2}$) with a rough bottom plate and a polycarbonate top lid (gap size $h = 1.5a$). In the presence of a vertical magnetic field B, particles repel each other with a force $\vec{F}_m$. The region of interest is of area $S = 5.7 \times 5.7\ \mathrm{cm^2}$.

*simon.merminod@univ-paris-diderot.fr

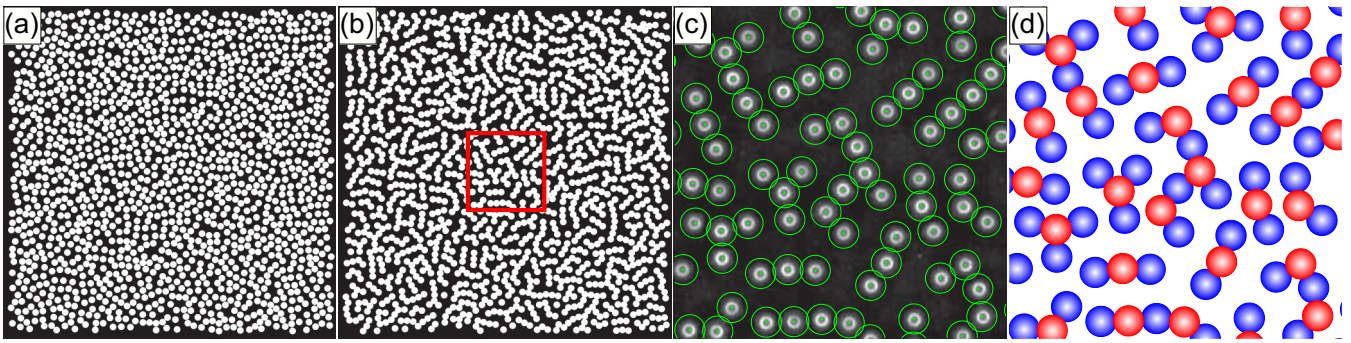

FIG. 2. (Color online) Top views of the system of particles. In (a) and (b), images of the spheres have been replaced by white disks of diameter a for better visualization, whereas (c) is from a direct image from the camera and (d) is the result of particle tracking. (a) Dissipative granular gas state at a moderate B (80 G). (b) Labyrinthine phase at a high B (170 G). The particles organize into an amorphous phase mostly composed of chains of a few particles. The region within the red square is enlarged in (c) and (d). (c) Thick circles are reflections of lighting on the spheres and appear smaller than the actual overlapping particle radii (thin circles). (d) Buckled chains (red spheres, top particles; blue spheres, bottom particles) mostly compose the amorphous phase.

II. FROM A GRANULAR GAS TOWARDS A LABYRINTHINE SOLID PHASE

The experimental setup is similar to the one used in [26]. Soft ferromagnetic spherical particles of diameter $a = 1$ mm are confined between two horizontal parallel plates separated by a gap of $h = 1.5a$ in order to form a monolayer as depicted in Fig. 1. Particles are vibrated vertically and are lit by an annular light-emitting diode (LED) array and imaged from the top by a fast camera through the transparent top plate. Particle center positions are tracked and their trajectories are reconstructed in the horizontal plane [21,27]. Interactions between particles are introduced by means of an external vertical magnetic field of amplitude B controlled by the experimentalist. Additional details on the experimental setup and protocol, and on the particle detection technique, are given in the Appendixes.

Magnetized soft ferromagnetic spheres behave as induced dipoles, whose magnetic moments are vertical and proportional to B. The interaction potential U_m of a particle located at a distance r and a polar angle θ from a second particle [28] reads in spherical coordinates [29], with μ_0 the vacuum permeability,

$$U_m(r,\theta) = -\frac{\pi}{16}\frac{B^2}{\mu_0}\frac{a^6}{r^3}(2\cos^2\theta - \sin^2\theta). \qquad (1)$$

Two spheres in the same horizontal ($\theta = \pi/2$) plane are thus repelling each other. Using this experimental method, macroscopic transitions were observed in 3D assemblies of magnetized soft-ferromagnetic particles [30,31]. Then the number of particles per surface unit is expressed by a dimensionless parameter, the area fraction $\phi = (N\pi a^2)/(4\,S)$, with N the number of particles tracked in the region of interest S. For a monolayer of particles, a high enough magnetic field, and a moderate area fraction ($\phi = 0.2$), the 2D granular gas solidifies into a hexagonal crystal [26], whose melting has been found to follow the Kosterlitz-Thouless-Halperin-Nelson-Young (KTHNY) scenario [32].

Here ϕ is increased to 0.5. For moderate values of the magnetic field B and continuous shaking, particles undergo a Brownian-like motion. At a given instant particle positions are random [Fig. 2(a)] and spheres exchange energy through dissipative collisions and magnetic interactions. We observe a 2D granular gas, whose properties are similar to those found at a lower area fraction [26]. Then by increasing B further, we observe that, despite the magnetic repulsion, small chains of two or three particles in contact start to form in the bulk of agitated particles. We remark also that the motions of the particles belonging to these chains are considerably restricted compared to those of free particles. At a higher magnetic field, the quasitotality of the particles are condensed into these chains [Fig. 2(b)]. At a large scale, the picture of the assembly of the system does not present an ordered structure. Thus, by increasing magnetic interactions, the system has been solidified in an amorphous state. Labyrinthine patterns were indeed described as globally disordered stripe domains [33]. Due to the presence of chains, the particle assembly presents striking similarities to the labyrinthine and stripe phases observed [16] and numerically predicted [10–14], for example, for 2D colloidal systems under thermal agitation and with dipolar repulsive magnetic interactions. Here, a transition from a granular gas phase to a labyrinthine phase for a macroscopic, out-of-equilibrium system is observed. This transition can also be visualized by applying a linearly increasing magnetic field from $B = 0$ G to $B = 200$ G (see video in Supplemental Material [34]). First, pairs aggregate, then triplets, and so on, homogeneously across the cell, until nearly motionless chains of various lengths occupy the whole cell, isolating the few remaining fluctuating particles from each other. We note also that, starting from the labyrinthine phase, the inverse transition is observed when the magnetic field is decreased. This shows that the system does not present any noticeable hysteresis.

By means of accurate particle tracking, chain morphology can now be quantitatively characterized. Chains are well separated due to the magnetic repulsion and can thus be considered as groups of more than one particle, according to a criterion of the contact distance. Moreover, chains appear mainly as linear objects because, most of the time, a particle inside a chain is in contact with two neighboring particles. Nevertheless, the relative orientations of the chains seem random. In the following, quantitative analysis of the small-scale structure reveals that chains correspond to a buckled

state of particles in contact [Fig. 2(c)]. A particle, once it is condensed in a chain, is in contact either with the top plate or with the bottom plate. Using slight differences in lighting for the two kinds of particles, our detection technique is able to provide the vertical position of the particles in the chains [as shown in the virtual image in Fig. 2(d)], which is coded as *up* (red spheres) or *down* (blue spheres). It can be noted that the particles at the tips of the chains are for the most part *down*, revealing an effect of gravity.

III. CHARACTERIZATION OF THE TRANSITION

Let us now quantitatively characterize the transition from a granular gas to the labyrinthine phase using the particle tracking data. The magnetic potential energy E_m and the horizontal kinetic energy E_c per particle can now be computed. From the interaction potential $U_m(r,\theta)$ defined in Eq. (1), the magnetic energy per particle is computed as the averaged summation over the pairs of the interaction potential of each pair,

$$E_m = \overline{\frac{1}{N_p}\sum_{i=1}^{N_p}\sum_{j=i+1}^{N_p} U_m(r_{ij},\theta_{ij})}, \tag{2}$$

with N_p the number of particles involved in the calculation of E_m; r_{ij} and θ_{ij}, respectively, the distance and the polar angle between the two particles i and j; and $\overline{\cdot}$ the temporal average. The magnetic potential energy depends on the local configuration of the particles, and therefore it fluctuates in time. Its averaged value, E_m, is found to be proportional to B^2 [Fig. 3(a)]. The kinetic energy per particle is computed from velocity measurements,

$$E_c = \tfrac{1}{2}\, m\, \overline{\left(\langle v_x{}^2\rangle + \langle v_y{}^2\rangle\right)}, \tag{3}$$

where m denotes the particle mass, v_x (respectively, v_y) the horizontal velocities in the x direction (y direction), and $\langle\cdot\rangle$ an ensemble average. E_c is a measure of the agitation in the system. When the magnetic field B is increased, in the first stage E_c grows [Fig. 3(b)]. Repulsive dipole-dipole interactions reduce the rate of dissipative collisions, which consequently increases E_c for a given shaking amplitude [26]. Once chains start to form, for $B \approx 100$ G, E_c drops significantly and nearly vanishes as the labyrinthine phase is formed for $B \approx 150$ G, illustrating the solidification process. For higher magnetic excitation values, the labyrinthine phase becomes less and less mobile as interactions strengthen and fluctuations are restrained.

Now, let us define the dimensionless control parameter $\varepsilon \equiv E_m/E_c$ [26], which is depicted as a function of B in the inset in Fig. 4(a). ε provides a measure of the competition between distance interactions and kinetic agitation. By analogy with an order parameter, the fraction of particles condensed in the chains φ is computed as the ratio of the number of particles belonging to a group of more than one particle to the total number of particles tracked in the region of interest. By plotting φ as a function of ε, as shown in Fig. 4(a), the transition is well depicted. For $\varepsilon < 60$, φ is nearly null in the granular gas phase, whereas for $\varepsilon > 1000$, φ is slightly smaller than 1, for the labyrinthine phase. The intermediate region of partial solidification corresponds to a coexistence zone between fluidized particles and particles condensed

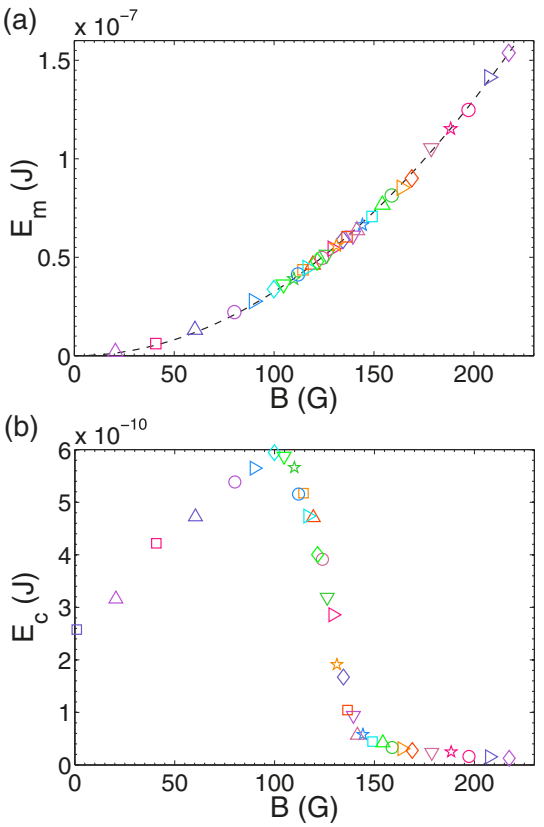

FIG. 3. (Color online) Potential magnetic energy and kinetic energy per particle. Each symbol corresponds to an independent experiment. (a) The potential magnetic energy is found to scale as B^2 (the dashed curve is a B^2 fit). (b) The kinetic energy, which measures agitation, plotted as a function of B. First, E_c increases due to the fluidizing effect of the magnetic interactions [26], then it suddenly drops towards 0 at the onset of solidification ($B \approx 100$ G).

in the chains. Let us emphasize that, although the simple criterion of the variation of φ captures well the transition from a granular gas to a labyrinthine phase, it should fail to distinguish a stripe phase from a labyrinthine phase. Topology and morphology would indeed have to be taken into account, like local orientational properties. Several approaches have been proposed to analyze or to model labyrinthine patterns, such as the introduction of a local wave vector [35], the computation of the wrinkledness [36], and the decomposition of the pattern into clusters of linear segments [33]. To our knowledge, the definition of an appropriate order parameter for labyrinthine patterns remains an open question.

Nonetheless, aiming at quantifying some of the directly observable morphological changes of the chains, we evaluate their mean length λ as a function of ε [Fig. 4(b)]. λ is defined as the average over all chains of the largest distance between particle centers inside a given chain. Starting from $1.6a$ at the formation of first chains, λ seems to saturate for the highest values of ε around $2.6a$. This suggests that competition between growing chains could limit their extension.

The pair correlation function, which is related to the probability of finding a particle center at a given distance from another particle center, provides information on the small-scale structure of the system. Before the transition, the particle

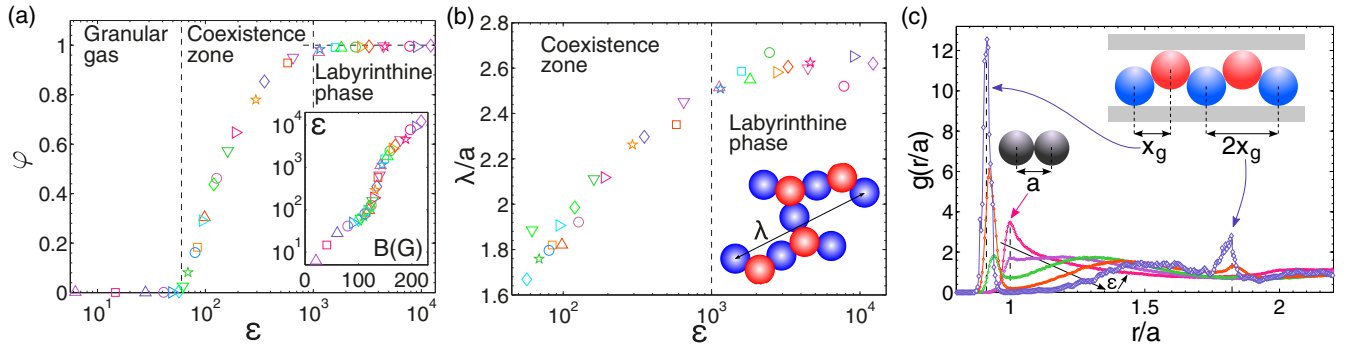

FIG. 4. (Color online) Characterizing the transition. Each symbol corresponds to an independent experiment. (a) The fraction of particles in chains φ as a function of the control parameter $\varepsilon = E_m/E_c$. It varies from about 0 in the dissipative state to 1 in the fully solidified state. The horizontal, dashed black line is a guide for the eye. Inset: ε as a function of B. (b) Adimensionalized mean chain length λ/a as a function of ε, with λ evaluated by computing the largest distance between particle centers inside a given chain. The value of λ averaged over the chains increases continuously with ε. If the averaging is weighted by the number of particles in the chains, the obtained values are larger by roughly 1 diameter unit, but the trend with ε is similar. (c) Evolution of the radial pair correlation function $g(r/a)$ for increasing values of ε (see arrow): $\varepsilon = 14.7$ (red), $\varepsilon = 41.0$ (purple), $\varepsilon = 68.9$ (green), $\varepsilon = 127$ (orange), and $\varepsilon = 649$ (blue). As the transition occurs, the $r = a$ peak of $g(r/a)$ drops down to 0, showing that the in-plane collision probability vanishes for high values of ε. In the meantime, another sharp peak appears at $r/a = x_g/a = 0.91$, which is the imprint of the buckled chains.

assembly evolves from a purely dissipative gas to an effectively more elastic gas [26]. Therefore, as Fig. 4(c) (red and purple lines) displays, the peak at the diameter value flattens while the effective elasticity rises. From the onset of solidification (green, orange, and blue lines), surprisingly, an extremely sharp peak grows from 0 at the distance value $r = x_g \approx 0.91a$, which is smaller than the particle diameter. This peak, which would be impossible to observe in purely 2D systems of hard spheres, reveals the internal structure of the chains. Here the gap size is indeed large enough so that partial overlaps of particles are allowed, leading to the formation of buckled particle chains in which particles are in contact with the top or bottom plate [see schematic in Fig. 4(c)]. Geometrical calculations yielding $x_g = \sqrt{2h\,a - h^2}$, one finds $h = 1.42$ mm, which corresponds to the announced gap of 1.5 mm diminished by the the roughness of the bottom plate. Moreover, in the labyrinthine phase (blue line), $g(r/a)$ also exhibits a shorter peak at the position $2x_g$, from the aligned second neighbors, showing the presence of linear chains. Between these two peaks, the zero probability at $x_g \lesssim r \lesssim 1.2a$ indicates the void spaces between the chains, while the nonvanishing probability for $1.2a \lesssim r \lesssim 2x_g$ stands for both nonaligned second neighbors in chains and particles from neighboring chains. The 3D effects related to the gap size h are thus essential to describe the small-scale structure of the labyrinthine phase. Therefore, we now discuss how three-dimensionality can explain the stability of the chains at a high enough area fraction.

IV. CHAIN FORMATION MECHANISM

At a low area fraction ($\phi = 0.2$ and lower), the stable state of the assembly of spheres in dipolar interaction was found to be a hexagonal crystal [26,32]. Why does the hexagonal structure now become unstable at a higher area fraction? How can we explain the formation of chains of particles in contact? In Fig. 5(a), we plot the 3D magnetic energetic landscape (in the vertical plane) for a sphere initially in the center of a hexagon of six neighboring particles, the projected horizontal distance between the particles being given geometrically by $d = a\sqrt{\pi/(2\sqrt{3}\phi)}$. Let us consider this central particle at $x = 0$ to be *up* [dashed circle in Fig. 5(a)] between six *down* neighbors, all at a distance d, and investigate its potential energy when it moves from $x = 0$ to the contact position for several values of ϕ [Fig. 5(b)]. Contact positions between spheres are local minima of potential energy, as the dipolar interaction aims to align spheres along a vertical axis. For $\phi = 0.2$, the central position is an absolute minimum of energy, in agreement with the expected stability of the hexagonal lattice. In contrast, when ϕ is increased, the energy barrier decreases and $E_m(0)$ augments relatively to $E_m(\pm d)$. For $\phi = 0.5$ contact positions become absolute minima, which can be reached by means of mechanical agitation. For $\phi = 0.6$, the central position is not even a minimum anymore. Therefore for $\phi = 0.5$ and above, we expect that the hexagonal structure is unstable, leading to local structures of spheres in contact like chains, despite the isotropic dipolar repulsion in a purely 2D system. This qualitative model explains the small-scale attraction leading to particle contacts, needed for the shaping and the stability of labyrinthine phases [8]. To improve the description, solid friction between the spheres and the top and bottom plates should be incorporated, as this may greatly stabilize the buckled chains. In thermal systems, similar predictions were obtained using Monte Carlo simulations [10–12]. In these examples and our system, the resultant of repulsive interactions of the assembly of particles over one acts as a magnetic pressure, favoring contact at a high enough particle density. Additionally, we note that buckled phases stabilized by pressure and friction can also appear in thin vibrated granular layers without magnetic interactions [37] if the density and gap size are sufficiently large [38]. Nevertheless, in the latter case, the structuring in separated chains is absent.

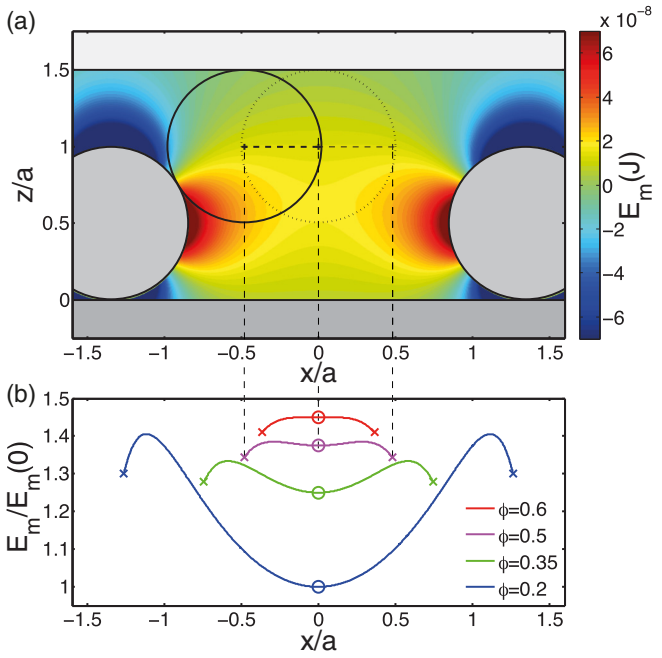

FIG. 5. (Color online) (a) The potential energy landscape E_m is computed for $\phi = 0.5$ and $B = 200$ G by averaging the pair potential U_m [see Eq. (1)] for six *down* neighbors forming a hexagon (four particles are out of the figure plane) and a central *up* particle moving along the x axis (dashed line). (b) The profile of E_m is plotted along this trajectory for four values of ϕ (curves have been rescaled and shifted vertically for clarity). The circles depict the initial central position and the crosses show the contact positions. From these graphs, for $\phi = 0.2$ and 0.35, hexagonal configurations are found to be stable, whereas for $\phi = 0.5$ and 0.6, the central particle in the presence of agitation should leave the position $x = 0$ to reach contact positions associated with buckled chains.

V. CONCLUSION

In this macroscopic and out-of-equilibrium model experiment, a labyrinthine phase is obtained by applying a magnetic field to a confined granular gas, by means of externally controlled dipolar interactions. We describe and quantitatively characterize the transition from a gas-like phase towards a globally disordered solid phase. It appears as a three-dimensional effect occurring in a quasi-two-dimensional system. The parameters setting the confinement, the gap h/a and the area fraction ϕ, are thus essential to explain the phase diagram of this granular medium, as also shown for colloidal and hard-sphere monolayers [12,16,39]. Although not presented here, after a fast increase in B, i.e., a magnetic quench, the labyrinthine phase exhibits a slow dynamics characterized by a slow evolution of its structural properties [40]. This aging phenomenon should thus be compared to the slow dynamics of structural glasses [41–43]. In the case of labyrinthine domain patterns arising in continuous systems, the analogy with glasses was also reported in an analysis of their globally disordered structure [33] and a study of their relaxation [36]. Finally, whereas the structure of the phases obtained in this macroscopic experiment resembles that of the phases found at thermal equilibrium in Monte Carlo simulations and colloidal monolayers [12,16,44], the kinetics of the transition described here is intrinsically an out-of-equilibrium process, which deserves further studies.

ACKNOWLEDGMENTS

The authors would like to thank Leonardo Gordillo, Jean-Claude Bacri, and Nicolas Vandewalle for discussions and Vincent Dupuis for performance of particle magnetization measurements. This work was supported by Université Paris Diderot and by the European Space Agency No. 4000103461CCN (Topical Team on granular materials).

APPENDIX A: POTENTIAL MAGNETIC ENERGY FOR TWO PARALLEL DIPOLES WITH FINITE MAGNETIC PERMEABILITY

For two ferromagnetic spheres of identical diameter a immersed in an unidirectional vertical magnetic field of intensity B and separated by a distance r, the potential energy of magnetic interaction reads in spherical coordinates as the interaction of two vertical magnetic dipoles [28],

$$U_m(r,\theta) = -\frac{\pi}{16}\frac{B^2}{\mu_0}\frac{a^6}{r^3}\left(\frac{\mu-\mu_0}{\mu+2\mu_0}\right)^2(2\cos^2\theta - \sin^2\theta), \tag{A1}$$

where θ is the polar angle between the two dipoles, $\mu_0 = 4\pi\,10^{-7}$ H $\cdot$ m^{-1} is the vacuum permeability, and μ is the intrinsic magnetic permeability of the sphere material. The induced magnetic fields of the neighboring particles are assumed negligible in front of the external magnetic field. For free-moving particles θ is taken equal to $\pi/2$, whereas for particles belonging to chains θ is computed from the measured vertical position of the particles (top or bottom). The magnetic potential energy per particle E_m is computed as an average of U_m over interacting pairs of particles [26] and in the limit of large μ. This approximation holds for soft and linear ferromagnetic materials [45], which is the case for our particles.

APPENDIX B: GENERATION OF THE VIBRATED AND INTERACTING SYSTEM OF PARTICLES

The particles are chromed alloy steel (AISI 52100) spheres of diameter $a = 1$ mm and of mass $m = 4.07 \times 10^{-3}$ g. Using a vibrating sample magnetometer, the magnetization of one particle was measured by V. Dupuis. The magnetic permeability μ verifies $122 < \mu/\mu_0 < \infty$ in the linear domain ($-2000\,\mathrm{G} < B < +2000\,\mathrm{G}$), and the remnant magnetic field B_r is below 12 G. The coercive field is small compared with the values of the magnetic field B used in our experiments. Within this range of B, the response to magnetic excitation is linear. The square aluminum cell (side, 9 cm long) containing these particles (see Fig. 1) is vertically driven by an electromagnetic shaker. The forcing is sinusoidal at the frequency $f_0 = 300$ Hz and the root mean square (RMS) acceleration of vibration is fixed at $\Gamma = 21.9\ \mathrm{m}\cdot\mathrm{s}^{-2} = 2.23g$ for all experiments, with g the gravity acceleration. This value corresponds to the upper limit of the linear response domain of the granular temperature $T_g = E_c/m$ as a function of Γ [21]. Two coils in Helmholtz configuration and current-controlled generate a nearly homogeneous magnetic field B across the cell (the measured variation is of 3%). Immersed in this magnetic field,

the particles are magnetized into induced dipoles vertically oriented (the particle rotation velocity is negligible compared with the speed of the magnetic domain rearrangements).

APPENDIX C: PARTICLE DETECTION

An annular LED array above the cell produces a high-contrast circular signal on the chromed particles, whose positions are recorded from above using a high-speed video camera at a high resolution (1152×1152 pixels at 780 Hz). The region of interest S is $5.7 \times 5.7\ \mathrm{cm}^2$ around the cell center (see Fig. 1). The particle diameter is about 20 pixels. For individual particle detection, we used a convolution-based least-squares fitting routine [21,46] completed by an intensity-weighted center detection algorithm (accuracy estimated as smaller than 0.3 pixel). Particle trajectories were reconstructed using a tracking algorithm [27,47].

APPENDIX D: EXPERIMENTAL PROTOCOL

The experimental protocol is fully automated for the sake of robustness. Every single experiment is noncorrelated with the others. The amplifiers of the electromagnetic shaker and of the Helmholtz coils are computer controlled via a data acquisition card. The experimental protocol routine is written in Matlab. It also proceeds to the dialogue with the camera, i.e., configuring and starting the video recordings, as well as to the recording of the data from the accelerometer and the Hall effect sensor. All experiments are performed according to the following protocol. First, the shaking is activated ($\Gamma = 21.9\ \mathrm{m \cdot s^{-2}}$) while the magnetic field remains 0. The magnetic field is then linearly increased (the rising rate $\alpha_q \equiv \mathrm{d}B/\mathrm{d}t$ is kept fixed for all experiments) up to its higher plateau value B. Afterwards, a waiting time is respected prior to proceeding to the recordings. It is chosen along with the recording time length so as to reach the chosen mean aging time τ_w. In all the experiments presented here, $\alpha_q = 1\ \mathrm{G \cdot s^{-1}}$, $\tau_w = 30$ s, and recordings last at least 2 s. Note that these two parameters, α_q and τ_w, have a noticeable influence on the nature of the labyrinthine state reached for high values of B, implying that a slow dynamics is at play.

For the 5000 particles introduced in the experiments, the area fraction evaluated on the cell is equal to 0.485. However, within the region of interest S, as the boundaries are not repulsive [26], ϕ decreases from 0.58 to 0.46 with B until $B \approx 80$ G. From the appearance of the first chains, ϕ remains nearly constant.

[1] M. Seul, L. Monar, L. O'Gorman, and R. Wolfe, Science **254**, 1616 (1991).
[2] M. Seul and M. J. Sammon, Phys. Rev. Lett. **64**, 1903 (1990).
[3] B. Sandnes, H. A. Knudsen, K. J. Måløy, and E. G. Flekkøy, Phys. Rev. Lett. **99**, 038001 (2007).
[4] B. Sandnes, E. G. Flekkøy, H. A. Knudsen, K. J. Måløy, and H. See, Nat. Commun. **2**, 288 (2011).
[5] A. Dickstein, S. Erramilli, R. E. Goldstein, D. P. Jackson, and S. A. Langer, Science **261**, 1012 (1993).
[6] F. Elias, C. Flament, J. C. Bacri, and S. Neveu, J. Phys. I France **7**, 711 (1997).
[7] K. J. Lee and H. L. Swinney, Phys. Rev. E **51**, 1899 (1995).
[8] M. Seul and D. Andelman, Science **267**, 476 (1995).
[9] K. De'Bell, A. B. MacIsaac, and J. Whitehead, Rev. Mod. Phys. **72**, 225 (2000).
[10] G. Malescio and G. Pellicane, Nat. Mater. **2**, 97 (2003).
[11] P. Camp, Phys. Rev. E **68**, 061506 (2003).
[12] J. Dobnikar, J. Fornleitner, and G. Kahl, J. Phys.: Condens. Matter **20**, 494220 (2008).
[13] Y. Shokef and T. C. Lubensky, Phys. Rev. Lett. **102**, 048303 (2009).
[14] M. D. Haw, Phys. Rev. E **81**, 031402 (2010).
[15] Y. Han, Y. Shokef, A. M. Alsayed, P. Yunker, T. C. Lubensky, and A. G. Yodh, Nature **456**, 898 (2008).
[16] N. Osterman, D. Babič, I. Poberaj, J. Dobnikar, and P. Ziherl, Phys. Rev. Lett. **99**, 248301 (2007).
[17] J. S. Olafsen and J. S. Urbach, Phys. Rev. Lett. **81**, 4369 (1998).
[18] J. S. Olafsen and J. S. Urbach, Phys. Rev. E **60**, R2468(R) (1999).
[19] W. Losert, D. G. W. Cooper, J. Delour, A. Kudrolli, and J. P. Gollub, Chaos **9**, 682 (1999).
[20] S. J. Moon, M. D. Shattuck, and J. B. Swift, Phys. Rev. E. **64**, 031303 (2001).
[21] P. M. Reis, R. A. Ingale, and M. D. Shattuck, Phys. Rev. E **75**, 051311 (2007).
[22] H. M. Jaeger, S. R. Nagel, and R. P. Behringer, Rev. Mod. Phys. **68**, 1259 (1996).
[23] D. L. Blair and A. Kudrolli, Phys. Rev. E **67**, 021302 (2003).
[24] A. Snezhko, I. S. Aranson, and W.-K. Kwok, Phys. Rev. Lett. **94**, 108002 (2005).
[25] L. Oyarte, P. Gutiérrez, S. Aumaître, and N. Mujica, Phys. Rev. E **87**, 022204 (2013).
[26] S. Merminod, M. Berhanu, and E. Falcon, Europhys. Lett. **106**, 44005 (2014).
[27] J. C. Crocker and D. G. Grier, J. Colloid Interface Sci. **179**, 298 (1996).
[28] J. D. Jackson, *Classical Electrodynamics*, 3rd ed. (Wiley, New York, 1998).
[29] See Appendix A for complements to the formula of U_m.
[30] C. Laroche and F. Pétrélis, Eur. Phys. J. B **77**, 489 (2010).
[31] D. Lopez and F. Pétrélis, Phys. Rev. Lett. **104**, 158001 (2010).
[32] J. Schockmel, E. Mersch, N. Vandewalle, and G. Lumay, Phys. Rev. E **87**, 062201 (2013).
[33] M. Seul, L. Monar, and L. O'Gorman, Philos. Mag. B **66**, 471 (1992).
[34] See Supplemental Material at http://link.aps.org/supplemental/10.1103/PhysRevE.92.062205 for a video of the transition.
[35] M. Le Berre, E. Ressayre, A. Tallet, Y. Pomeau, and L. Di Menza, Phys. Rev. E **66**, 026203 (2002).
[36] B. Reimann, R. Richter, and I. Rehberg, Phys. Rev. E **65**, 031504 (2002).

[37] P. Melby, F. V. Reyes, A. Prevost, R. Robertson, P. Kumar, D. A. Egolf, and J. S. Urbach, J. Phys.: Condens. Matter **17**, S2689 (2005).
[38] In our cell with $h = 1.5a$, the total number of particles should be larger than 9477 for such a buckled state to be observed [37].
[39] M. Schmidt and H. Löwen, Phys. Rev. E **55**, 7228 (1997).
[40] The slow dynamics reported in some attractive granular gases [23,25] results from a cluster growth process and should not be described as an aging phenomenon.
[41] J. Barrat and J. Hansen, *Basic Concepts for Simple and Complex Liquids* (Cambridge University Press, Cambridge, UK, 2003).
[42] G. L. Hunter and E. R. Weeks, Rep. Prog. Phys. **75**, 066501 (2012).
[43] F. H. Stillinger and P. G. Debenedetti, Annu. Rev. Condens. Matter Phys. **4**, 263 (2013).
[44] R. Messina, S. Aljawhari, L. Bécu, J. Schockmel, G. Lumay, and N. Vandewalle, Sci. Rep. **5**, 10348 (2015).
[45] A. Mehdizadeh, R. Mei, J. Klausner, and N. Rahmatian, Acta Mech. Sin. **26**, 921 (2010).
[46] M. D. Shattuck, Particle tracking. Available at: gibbs.engr.ccny.cuny.edu/technical/Tracking/ChiTrack.php; accessed 18 April 2013.
[47] J. C. Crocker and E. R. Weeks, Particle tracking using idl. Available at: www.physics.emory.edu/faculty/weeks/idl/; accessed: 18 April 2013.